INL/JOU-23-75804-Revision-0

Recent progress on understanding the temperature-dependent irradiation resistance ranking among NiFe, NiCoCr and NiCoFeCr alloys: A review

G. Velisa, F. Granberg, E. Levo, Y. Zhou, Z. Fan, H. Bei, F. Tuomisto, K. Nordlund, F. Djurabekova, W. J. Weber, Yanwen Zhang

Changing the World's Energy Future

Idaho National Laboratory

INL is a U.S. Department of Energy National Laboratory operated by Battelle Energy Alliance, LLC

INL/JOU-23-75804-Revision-0

Recent progress on understanding the temperature-dependent irradiation resistance ranking among NiFe, NiCoCr and NiCoFeCr alloys: A review

G. Velisa, F. Granberg, E. Levo, Y. Zhou, Z. Fan, H. Bei, F. Tuomisto, K. Nordlund, F. Djurabekova, W. J. Weber, Yanwen Zhang

February 2023

Idaho National Laboratory
Idaho Falls, Idaho 83415

http://www.inl.gov

Prepared for the
U.S. Department of Energy
Under DOE Idaho Operations Office
Contract DE-AC07-05ID14517

Recent progress on understanding the temperature-dependent irradiation resistance ranking among NiFe, NiCoCr and NiCoFeCr alloys: A review

G. Velişa[1,2,a)], F. Granberg[3], E. Levo[3], Y. Zhou[1], Z. Fan[1], H. Bei[4], F. Tuomisto[5], K. Nordlund[3], F. Djurabekova[3,5], W.J. Weber[4], and Y. Zhang[1,4,6,a)]

[1]Materials Science and Technology Division, Oak Ridge National Laboratory, Oak Ridge, TN 37831, USA
[2]Horia Hulubei National Institute for Physics and Nuclear Engineering, P.O.B. MG-6, 077125 Magurele, IF, Romania
[3]Department of Physics, University of Helsinki, P.O.B. 43, 00014 Helsinki, Finland
[4]Department of Materials Science & Engineering, University of Tennessee, Knoxville, TN 37996, USA
[5]Helsinki Institute of Physics, University of Helsinki, P.O.B. 43, 00014 Helsinki, Finland
[6]Energy and Environment Science & Technology, Idaho National Laboratory, Idaho Falls, ID 83415, USA
[a)]Address all correspondence to these authors. e-mails: gihan.velisa@nipne.ro; Yanwen@utk.edu

Abstract

Systematic temperature-effects investigations on damage evolution in ion-irradiated Ni-based concentrated solid-solution alloys (CSAs) are pivotal to provide reliance on their use in nuclear applications. In search of the origin behind the temperature-dependent irradiation resistance ranking among equiatomic NiFe, NiCoCr and NiCoFeCr alloys, we have compared, previously experimental and theoretical published data involving ion irradiation experiments performed on these alloys with new ion channeling results from ion-irradiated NiCoFeCr at 500 K. Moreover, the current results are compared with independent theoretical calculations and relevant TEM results from literature, which allow us to suggest that the lower migration energy of vacancies in NiCoCr, as compared with those in NiFe and NiCoFeCr, is the reason behind why NiCoCr is no longer outperforming NiFe under ion irradiation above 300 K.

Keywords: Concentrated solid-solution alloys, Ion irradiation, Vacancy mobility, Irradiation temperature

1. Introduction

The development of materials that are able to perform better than traditional alloys under extreme environments (e.g., high irradiation doses, high temperatures, etc.) has been long pursued[1,2] and still draws intense attention and boosts research efforts in the nuclear materials engineering community[3,4]. For nearly two decades, a new class of alloys, namely concentrated solid-solution alloys (CSAs)[5,6], has been on the radar of the material science community due to a unique combination of properties (e.g., exceptional mechanical properties[7–9], improved corrosion[10] and thermomechanical[11] performance); moreover, since then, improved radiation resistance has been discovered in some CSAs, making them possible candidate materials for nuclear applications[12–15]. Since tailoring the composition and microstructure of CSAs may enable a further improvement of these highly desirable properties in operating conditions of nuclear materials, interests in understanding the effects of chemical complexity on the irradiation response of CSAs have grown exponentially in the last few years[16–22]. Here one should note that CSAs family includes both medium-entropy alloys (MEAs, e.g., with three alloying elements [18]) and high-entropy alloys (HEAs, e.g., with five or more alloying elements [5,6,23]).

In contrast to traditional alloys (solvent–solute alloys), CSAs are mixtures of metallic elements in which the atoms, in equiatomic or large non-equiatomic proportions, are randomly distributed on structurally simple lattices (e.g., FCC or BCC) [8,12,13,24–26]. Recent studies have revealed that the random arrangement of multiple species is the origin of the extreme chemical disorder [14,25,27,28] and complex energy landscapes [24,25,29] found in CSAs. It has further been shown that this random arrangement may be highly effective for altering mass transport and radiation damage processes[17]. Exploiting the local chemical complexity of CSAs may be the more gainful path for improving physical and chemical properties (e.g., mechanical, corrosion and radiation resistance) that are highly desired for space and nuclear applications. These findings have stimulated us to perform studies on the exploration of

chemical alternation effects on irradiation-induced damage evolution in CSAs at room-temperature (300 K). *In-situ* Rutherford backscattering spectrometry in channeling conditions (RBS/C) has been frequently employed to study irradiation-induced damage accumulation in some CSAs (Ni, NiCo, NiFe, NiCoCr and NiCoFeCr) at 300 K [4], because RBS/C is sensitive to various types of defects, such as uncorrelated displaced lattice atoms (e.g., point defects, clusters of point defects, amorphous clusters) and extended defects (e.g., dislocation loops and stacking fault tetrahedra (SFT)), and also to lattice distortion [30–35]. Thus, useful insight into the depth-dependent damage accumulation and evolution processes as a function of ion fluence (or dose) can be obtained by RBS/C. Moreover, RBS/C provides good statistical information on disorder, complimentary to some other techniques, such as transmission electron microscopy (TEM) that provides very local but detailed microstructural information[4]. In addition, molecular dynamics (MD) simulations in conjunction with RBS/C studies have demonstrated that the diffusion of large vacancy clusters, such as stacking-fault tetrahedral, is much slower in CSAs (i.e., $Ni_{50}Fe_{50}$, $Ni_{80}Fe_{20}$, $Ni_{80}Cr_{20}$, and $Ni_{40}Fe_{40}Cr_{20}$) than in elemental Ni[36]. Our previous RBS/C studies[14,24] have shown that increasing lattice disorder in these CSAs (Ni, NiCo, NiFe, NiCoCr and NiCoFeCr) strongly delays damage accumulation. For example, these materials rank in the order of decreasing damage accumulation rate as Ni > NiCo > NiFe > NiCoCr ≈ NiCoFeCr[18]. Additional MD simulations have shown that, with increasing lattice disorder in CSAs, the migration pathways of dislocations are limited. Therefore, the growth of stable extended defects is strongly hindered, resulting in a decreased damage accumulation rate, as determined by RBS/C. These findings call for attention to understand the chemical complexity effect on defect evolution at the early stages. This may be the more profitable pathway for designing high-performance nuclear materials, since the suppressed damage evolution at the early stages may consequentially result in improved radiation resistance[15,17].

For their use in nuclear applications, the response of CSAs to high irradiation doses performed not only at room-temperature but also at high-temperatures should be investigated. Thus, our research group has further focused on the exploration of chemical alternation effects on radiation-induced segregation (RIS) [15,37–39] and void swelling response [15,40–43] of Ni-based CSAs (Ni to NiCoFeCrX (X = Mn or Pd)). Some of these studies [40,41] have shown that increasing compositional complexity in CSAs strongly enhances the void swelling-resistance of these alloys. These experimental studies complemented by MD simulations have shown that, with increasing compositional complexity in CSAs, a transition from 1D long-range migration to random 3D short-range diffusion of small interstitial clusters occurs. It is believed that the 3D motion observed in complex alloys (such as NiFe and NiCoFeCr) enhances the interactions between interstitials and vacancies, facilitating dynamic annealing of these defects at early stages during irradiation, which in turn results in enhanced swelling resistance [44,45]. In contrast, 1D long-range migration observed in Ni, NiCo and some dilute alloys [45] may facilitate the growth of large clusters, resulting in poor swelling resistance. Zhang et al. [43] have demonstrated that 3*d*-electrons effectively alter energy dissipation, transport properties, defect energetics, defect survival and interstitial migration pathways [15,43]. The work further reveals that these defect processes are affected by expanding the number of constituent metal species with large variances in number of 3*d*-electrons. The effective dynamic annealing is, therefore, much more pronounced in alloys that incorporate metal species with large variances in 3*d*-electrons. There are additional studies that have focused particularly on the comparison of radiation-induced void swelling in HEA and conventional alloys. These studies have shown that conventional alloys possess lower void swelling resistance in comparison to HEAs (a subset of CSAs) [46–48].

Previous research [37,38] has also examined the chemical alternation effects on the RIS process in CSAs and demonstrated that the RIS level decreases with increasing compositional complexity due to sluggish atom diffusion. Later [45], it was demonstrated that there is a

correlation between RIS level and chemically biased mass and defect transport that results from d-electron effects. One of these studies [37] has also shown that the magnitude of RIS in some CSAs is lower in comparison to conventional alloys. In the past years, the fundamentals of damage formation in HEAs irradiated at room- and high-temperature to medium and high fluences have also been intensively studied [49,50,59–68,51–58]. Some of these studies focused on the comparison of RIS in HEAs and conventional austenitic stainless steels [49,52]. For example, Kumar et al. [49] shows that the FeNiMnCr HEA manifest an enhanced RIS-resistance compared to Fe-Cr-Ni alloys [69] irradiated under similar conditions, which was attributed to sluggish diffusion. This same experimental study reveals that the peak segregation in HEAs occurs at higher irradiation temperatures (between 500 and 700°C) compared to conventional austenitic steels (between 300 and 500 °C [69,70]). Recently, experimental studies [52,62] revealed that the inverse Kirkendall effect is the primary RIS mechanism in CoCrFeMnNi. Previous bulk tracer diffusion experiments support that inverse Kirkendall effect is the primary mechanism RIS in NiCoFeCr and NiCoFeCrMn [71]. Allen et al. [69] postulated that the inverse Kirkendall effect is the primary RIS mechanism in austenitic Fe-Cr-Ni alloys.

Systematic temperature-effects investigations on damage evolution in ion-irradiated Ni-based CSAs (NiFe and NiCoCr) have revealed one of the most intriguing findings: the relative irradiation resistance of these alloys as a function of temperature inverts with increasing temperature[72,73]. In these studies, we showed that the radiation performance of NiCoCr is better than NiFe under ion irradiation at temperatures ≤300 K; however, the ranking of radiation performance (swelling resistance) is reversed for ion irradiation performed at temperatures >300 K (i.e., 773 K) [40]. The origin of this intriguing temperature-dependent mechanism is not yet well-understood, although it has been speculated that the NiCoCr alloy has smaller differences in d-electrons than the NiFe alloy, resulting in an increased capability to dissipate incident energy and higher electron mean free paths. This in turn results in a degradation of the defect recombination and annihilation efficiency (i.e.,

"self-healing" effect). More recently, both simulated RBS/C results by Levo et al.,[74] and experimental RBS/C results by Velisa et al.[72] showing a lower backscattering yield for NiCoCr and NiFe compared to Ni support the conclusion that the 3d electron configurations in CSAs play a crucial role in determining the irradiation resistance. One can argue with such an assumption, since temperature shouldn't directly affect the 3d electron configurations and thus alone cannot account for such inversion of irradiation resistance ranking.

In order to shed light on understanding the origin of this intriguing temperature-dependent irradiation resistance ranking, ion channeling was employed to study damage evolution in NiCoFeCr irradiated at 500 K and compared with previous ion channeling analysis performed on ion-irradiated NiFe[73] and NiCoCr[72] at 300 K and 500 K. In conjunction with independent theoretical calculations, unlike previous studies, the underlying mechanism for temperature-dependent irradiation resistance ranking are discussed. So far it is believed, that the lower migration energy of vacancies in NiCoCr, as compared with those in NiFe and NiCoFeCr, is the reason behind why NiCoCr is no longer outperforming NiFe under ion irradiation performed at elevated temperatures (i.e., 500 K) has been obtained from ion channeling results. It is concluded, that at this temperature vacancies become mobile, influencing defect dynamics and ultimately leading to the aggregation of larger vacancy clusters in NiCoCr than in NiFe and NiCoFeCr.

2. Experimental Results

The RBS/C spectra collected for NiCoFeCr irradiated at 500 K with 1.5 MeV Ni ions to seven fluences (8, 10, 13, 40, 80 and 150 Ni^{+}/nm^{2}, respectively), are illustrated in Fig. 1(a). To define the amorphous and undamaged levels, the random and <100>-aligned spectra from an unirradiated (pristine) area, respectively, are also included in Fig. 1(a). The channeling spectrum collected from pristine sample exhibit a much lower yield than the random one. The value of the axial minimum yield, χ_{min} ~0.05, obtained for the Ni sublattice below the surface peak proves the high quality of the NiCoFeCr single crystals used for this study. The Ni-

irradiated channeling spectra illustrated in Fig. 1(a) are characterized, as compared to that for unirradiated samples, by a higher backscattering yield, which increases with increasing ion fluence (at least up to 40 Ni^+/nm^2) due to the accumulation of irradiation damage. Additional irradiation to ion fluences from 40 to 80 ions Ni^+/nm^2 and to 150 Ni^+/nm^2, the backscattering yield is no longer increases. This indicates that the saturation of the relative damage level occurs at fluences between 40 to 80 Ni/nm^2. Here one should note that the aligned spectrum recorded on the Ni-irradiated sample at the highest ion fluence (150 Ni^+/nm^2) does not reach the random level, indicating that the loss of crystallinity or full amorphization is not occurring based on the RBS/C criteria. It is also worth mentioning the Ni-irradiated channeling spectra illustrated in Fig. 1(a) are characterized by a high dechanneling background, leading to the emergence of the knee-like structure. In other words, the RBS spectra acquired along the <100>-axial direction on Ni-irradiated areas do not exhibit clear damage peaks. This presumably relates to the presence of extended defects (i.e., dislocation loops and SFT) in the irradiated layer, as previously concluded by multi-energy ion channeling measurements performed on pure Ni[75] and NiCoFeCr[76] irradiated at 300 K. The formation of extended defects in NiFeCoCr irradiated at 500 K is confirmed based on MD simulations (see discussion below), which is consistent with previous independent *in-situ* TEM analysis carried out on NiCoFeCr under 1 MeV Kr ion irradiation at 773 K [77].

Analysis of the RBS/C spectra depicted in Fig. 1(a) yields the depth dependences of relative disorder, which are illustrated in Fig. 1(b). For visual clarity, only best fits to experimental data are depicted in Fig. 1(b). The results in Fig. 1(b) clearly reveal that there is a constant increase in irradiation-induced disorder at the damage peak with increasing fluence, up to a fluence 40 $ions/nm^2$. Above this fluence, the disorder saturates, and the peak in apparent disorder shifts to greater depths as the ion fluence increases from 40 to 150 Ni^+/nm^2. The saturation of the relative damage level occurs at fluences between 40 to 80 $Ni^+//nm^2$. Similar values of critical ion fluence to induce saturation of relative disorder are also reported

for other ion-irradiated CSAs at 500 K, such as NiFe [73] and NiCoCr [72]. In the fluence range before saturation (from 5 to 40 Ni^{+}/nm^{2}), a good correlation between measured damage profiles and SRIM-predicted dpa profile is observed. One should also note that, up to the maximum fluence of 150 ions/nm^{2} in this study, an amorphous phase is not produced. It is worth noting that once the accumulated ion fluence goes above 80 $Ni^{+}//nm^{2}$, the maximum disorder starts to move beyond the peak damage production region where the most intense collision cascades occur due to the development of irradiation-induced stresses (see discussion below) [34,78], which is consistent with previous independent *ex-situ* TEM analysis carried out on fcc CSAs (i.e. 3 MeV Au-irradiated NiFe and NiCo at 300 K)[78]. Here, it is also worth mentioning that the extracted depth profile of (defect size) x (defect density) from TEM observations are in good agreement with the disorder profiles extracted using iterative procedure (IP).

3. Discussion

3.1. Dose dependence of early stages damage evolution: 300 vs. 500K

The damage evolution may be quantified by plotting the irradiation-induced disorder at the damage peak with increasing dose or fluence, as illustrated in Fig. 2 (b), where the increase in the relative disorder at the initial damage peak, at early stages (low-dose irradiation cases), is shown as a function of ion dose for NiCoFeCr (green filled triangles) irradiated with 1.5 MeV Ni ions at 500 K. The dose dependence of relative disorder at the damage peak for NiFe[73] (blue filled circles) and NiCoCr[72] (red filled squares) irradiated under identical conditions are superimposed for comparison. In order to see how both the local chemical environment and irradiation temperature influences the early stages of damage production and cluster formation in complex CSAs, previous experimental studies on damage evolution in NiFe[73] (blue filled circles), NiCoCr[72] (red filled squares) and NiCoFeCr[76] (green filled triangles) irradiated with 1.5 MeV Ni ions at 300 K are summarized in Fig. 2 (a). Note that the initial damage peak is situated at depths of about 375, 417 and 424 nm in NiFe[73],

NiCoCr[72] and NiCoFeCr[76], respectively. At early stages (low-dose irradiation cases), damage evolution exhibits a linear dependence on dose, as indicated by the linear fits to the experimental data (see dashed lines) for NiCoCr and NiCoFeCr irradiated at 300 K (Fig. 2(a)), up to 1.17 and 1.42 dpa for NiCoCr and NiFeCoCr, respectively. On the other hand, the disorder accumulates slowly at the beginning of irradiation (between 0 and 0.12 dpa) and then increases rapidly before saturation (0.42 dpa), giving rise to the well-established superlinear shape of the damage evolution curve[79]. In other words, these damage accumulation curves can be divided into two groups i.e., linear (NiCoCr and NiCoFeCr) and superlinear (NiFe) dependence on dose. It is well-known that such a superlinear dependence results from the overlapping of a large number of defects, while a linear dependence suggests less overlapping of defect production in NiCoCr and NiCoFeCr than for NiFe[21]. This indicates that a higher number of defects per incident ion is produced in NiFe than in NiCoCr and NiCoFeCr under 1.5 MeV Ni ions irradiation at 300 K.

The different damage accumulation behavior of NiFe compared to NiCoCr and NiCoFeCr observed by RBS/C is also confirmed by the positron annihilation spectroscopy (PAS) signals recorded on NiFe, NiCoCr and NiFeCoCr irradiated at 300 K using Ni ions with multiple energies (2, 4, 8 and 16 MeV) at various ion doses (ranging from 0.01 to 1 dpa)[29,39]. The PAS signals are usually characterized with shape parameters S and W that quantify the contribution from valence electrons and from core electrons, respectively[80]. Briefly, S and W parameters are sensitive to open volume defects and to the chemical environment surrounding the annihilation site. For example, the generation of vacancy defects results in an increase of the S parameter. In other words, the amplitude of the S and W parameters are fingerprints of the irradiation-induced disorder since samples with the lowest defects will be characterized by lower S-parameter and higher W-parameter [80]. The parameters S and W recorded on the irradiated alloys are shown in Fig. 3 as a function of the irradiation dose, together with the PAS signals from unirradiated NiFe, NiCoCr, and

NiFeCoCr defining the reference points for the lowest S and the highest W values. These reference points define the samples with lowest concentration of native defects. Looking at these reference points, it is clearly seen that NiFe has the highest value of S parameter, then comes NiFeCoCr, and last comes NiCoCr. This presumably reflects that, among all three alloys, the highest fraction of positrons trapped at open-volume native defects is in NiFe [39]. Compared with these reference points, PAS signals from the irradiated alloys are characterized by higher and lower S and W values, respectively. Although similar dose dependence (S and W parameter values decreases and increases with dose, respectively) is observed for all three alloys up to 0.3 dpa, these signals appear into two groups i.e., lower (NiCoCr, and NiFeCoCr) and higher (NiFe) S and W parameters, as indicated by the transparent rectangle covering the *S* - *W* data sets of NiFe. With further increasing ion dose from 0.3 to 1 dpa, the initial trend is kept for NiCoCr and NiCoFeCr; on the other hand, the value of the S parameter increases, but the value of W decreases for NiFe, as indicated by the black arrow. This may indicate that the vacancy-type defect production and evolution reach saturation in NiFe between 0.3 and 1 dpa, while the damage build-up continues in NiCoCr and NiFeCoCr.

Compared with room-temperature results, the early stages of damage evolution (see dashed lines in Fig. 2(b)) in NiFe, NiCoCr and NiCoFeCr irradiated at 500 K, shows a linear dependence on dose, for all three alloys. It is important to note that the early stages of damage evolution under 500 K shifts to much higher ion doses compared to 300 K. This is not surprising since raising the irradiation temperature, the dynamic recovery during irradiation due to thermally-enhanced processes (defect migration and defect clustering) becomes more and more dominant. It is also worth remarking that the disorder evolution vs. dose at 500 K (Fig. 2(b)) shows slopes between 0.03 and 0.04, while the dependence of damage evolution on dose follows a slope of ~0.1 for both NiCoCr and NiCoFeCr irradiated at 300 K (Fig. 2 (a)). Higher slope indicates that the damage accumulation process is faster. This is another

piece of evidence that the damage accumulation process is slower at 500 K than at 300 K due thermally-enhanced dynamic annealing process. One of the most intriguing outcomes from this comparison is that the relative disorder in NiFe is slightly lower than that in NiCoFeCr and even lower than in NiCoCr irradiated at 500 K up to 5 dpa. In addition, the damage accumulation curve (linear dependence on dose) of NiFe exhibits the lowest slope among all alloys, indicating that the early stage of damage evolution is slower. These findings demonstrate that NiFe exhibits a more favorable chemical environment for suppressing early stage damage accumulation under high temperature irradiation than the NiCoCr. Suppression of damage accumulation at early stages is expected to inhibit deleterious microstructural changes at late stages.

The deviating defect accumulation curve of NiFe from linear dependence on dose, as shown in Fig. 2(a), can be understood by taking into consideration the thermal conductivity values and *e–ph* coupling strengths. As discussed and illustrated in detail elsewhere[14,15,21], the post-ballistic recovery is enhanced in CSAs alloys with lower thermal conductivity (or higher electrical resistivity) and stronger *e–ph* coupling, which results in more localized heating (greater thermal 'spike' temperature for prolonged time) and subsequent defect recombination capacity (smaller defect clusters). Indeed, among the three alloys, the room-temperature electrical thermal conductivity of NiFe (21.1 $W\,m^{-1}\,K^{-1}$) is higher than that of NiCoCr (7.2 $W\,m^{-1}\,K^{-1}$) and NiCoFeCr (8.0 $W\,m^{-1}\,K^{-1}$)[81]. The difference in defect accumulation response, illustrated in Fig. 2(a), between the two groups (NiCoCr and NiCoFeCr vs. NiFe) can also be justified by taking into account the limited migration pathways of dislocations arising from the intrinsic lattice distortion of disordered alloys. Indeed, the existence of smaller defect clusters in NiCoCr than in NiFe under ion irradiation at temperatures ≤ 300 K and, more importantly, their less likely growth due to limited dislocation mobility has been predicted theoretically and experimentally confirmed from TEM micrographs recorded on NiFe and NiCoCr irradiated with 1.5 MeV Ni ions at 300 K[82]. Another reason for the observed

irradiation resistance ranking at 300 K is the theoretical calculations that predict a larger overlapping region between the migration energies of vacancies and interstitials in both NiCoCr and NiCoFeCr compared to NiFe[21]. The larger region of overlap in their migration barrier distributions may additionally contribute to enhanced defect annihilation.

The MD results are now discussed in more detail. First, looking at the early stages of damage build-up, we can observe the same trend for all materials and temperatures, a linear increase of defects, when no overlap is happening. As the overlap effects are starting to take place, a sub-linear increase is seen in the defect numbers. Even though different interatomic potentials show different quantitative results, these following trends are observed. At higher doses, we can observe that Ni contains much more defects than the two other alloys. At 300 K, it is seen that NiFe show more defects than NiCoCr[82,83], but at the higher temperatures, the difference is not as clear[74]. The defect concentration as a function of dose is shown in Fig. 4, where we can see the initial linear regime and the transition to the sub-linear regime, as well as the cross-over in Ni behavior from showing the least damage to showing the most. We can also observe that at 300 K there is a difference between materials, but at 500 K and 800 K, it is quite similar. As shown in Ref. [74], at the highest doses achieved by MD, we can see that saturation of defects or a transition to very minor increases in defect concentration are happening at doses between 0.1 to 0.3 dpa. On a general level, the higher the temperature the lower the number of defects and number of dislocations.

Looking at the dislocation evolution in Fig. 5 (a)-(i), we can observe that, for all three temperatures before the crossover, Ni exhibits the least number of dislocations. Mainly partial dislocation loop networks are seen for all materials, and additionally some stair-rod dislocations are seen in Ni, which are a precursor to formation of SFT. The loop sizes are slightly larger for Ni than for the other materials, which is also reported in the supplementary material of Ref.[74], where larger interstitial clusters are formed at lower dose in Ni compared to the alloys. At the crossover (see Fig. 6 (a)-(i)), a similar trend is observed as before the

crossover, where Ni exhibits the least number of dislocations, but the sizes are larger. The same kind of dislocations are observed, except occasionally a Frank loop forms in Ni. However, the number of stair-rod dislocations and SFT are increasing in Ni. After the crossover (see Fig. 7 (a)-(i)), we can see that in Ni there exist mainly a single large Shockley partial dislocation loop or a Frank loop, and a large amount of SFT. In the other materials, mainly a few intermediate sized Shockley partial loops and a large amount of small Shockley partial loops are observed. The main difference is that the SFT are vacancy type, which stabilizes the vacancies into clusters in Ni; whereas in the alloys, the vacancies are in more random clusters. These vacancy clusters are of similar sizes according to the supplementary material in Ref.[74], but the stability and effect on overlapping cascades are likely different. Among the alloys, larger defects are observed in NiCoCr than in NiFe, with increasing irradiation temperature.

3.2. Comparison of defect accumulation at late stages*: 300 vs. 500 K*

Fig. 8 presents the damage accumulation in NiFe, NiCoCr and NiCoFeCr irradiated with 1.5 MeV Ni ions at (a) 300 K and (b) 500 K. Although at first glance, the relative disorder at the initial damage peak increases towards saturation with increasing ion dose and then decreases, independent of alloy composition and irradiation temperature; yet composition and temperature influence both the damage accumulation rate towards the saturation level and threshold dose for the onset of saturation level. For example, the threshold dose for the onset of saturation level (marked with arrows) increases with both increasing irradiation temperature and chemical complexity. The damage accumulation behavior in NiFe and NiCoCr found in the modeling work has shown that, at early stages of damage formation, point defects and small clusters are produced, similar to that revealed in independent ex- and in-situ TEM analyses of NiFe, NiCoCr and NiCoFeCr irradiated at 300 [14,82] and 773 K[77]. The formation of point defects and small defect clusters in collision cascades during Ni ion irradiation may be responsible for the weak dependence of relative disorder [83,84]. Previous MD

simulations[82,85] have revealed an increase of volumetric strain at low doses due to the production of point defects and small clusters; while an relaxation of strain is observed at higher doses, which is associated with the transformation of small defects into large defect clusters[85]. Here, one should note that the diffusion of point defects is enhanced with increasing irradiation temperature; [86–88] thus the probability of point defects absorption by the sinks originally existing in the material increases [46,67]. Whereas, the surviving point defects may further aggregate into more stable and larger defect clusters (e.g., SFT) via diffusion and migration progress [60,63].

Under further ion irradiation, damage accumulation curves show a sublinear increase with ion dose to saturation. Defect clustering analysis of the MD simulations reveals that, with the increasing number of overlapping cascade damage, small clusters grow in size and then aggregate into ordered defect structures, such as partial and perfect dislocation loops, similar to that revealed in independent ex- and in-situ TEM analyses of NiFe, NiCoCr and NiCoFeCr irradiated at 300 [14,82] and 773 K[77]. Looking at these damage accumulation curves, it is clear that NiFe saturates at a lower ion dose than NiCoCr and NiCoFeCr, independent of the irradiation temperature. While the critical dose for saturation under 1.5 MeV Ni ions irradiation at 500 K is lower for NiFe than NiCoCr and NiCoFeCr, a slower damage accumulation rate for NiFe, as compared with damage evolution in NiCoCr, is observed, as indicated by the steeper slopes for damage accumulation in NiCoCr and NiCoFeCr (see Fig. 8(b)). One should note that the relative disorder level in NiFe saturates at a value of 0.20, which is lower to that observed in NiCoCr (0.29) and NiCoFeCr (0.23). In a previous experimental study on the influence of temperature on disorder evolution in irradiated NiCoCr [72], it has been shown that the mean relative disorder in this ternary alloy irradiated at 500 K saturates at a higher disorder value than at 300 K. In contrast, the magnitude of residual damage in NiCoFeCr irradiated at 500 K saturates at a lower disorder value (~0.23) than at 300 K (~0.32). More damage at a higher temperature means that the thermal processes active

during the irradiation at 500 K are not sufficient to drive defect recovery in NiCoCr, but on the contrary led to microstructural modifications. One would therefore suspect that a second type of defect is formed by a process that is enhanced in NiCoCr irradiated at 500 K. Note that, for the NiCoFeCr alloy, the recrystallization process occurs above 700 K [89]. Levo et al. [83] have shown that the saturated defect amount is dependent on alloy composition. This same theoretical study has also revealed that there is a linear correlation between the saturated defect concentration and their corresponding dislocation mobilities. However, due to the lack of defect sinks in the simulations, the very low dislocation mobility, which can induce lower defect concentration, can lead to the retention of defects at higher temperatures. For example, the practically immobile dislocations at low temperatures lead to less defect build-up due to decreased interaction of dislocations, yet they can induce dislocation retention at high temperature. However, in materials where dislocations are mobile, they can annihilate at defect sinks. This could explain the observed experimental trend of the opposite behavior at the increased temperature.

Finally, the magnitude of residual disorder shows a transition from an damage accumulation stage to a saturation stage, followed by a stage of decreasing disorder. The continuous growth of relatively small dislocation loops to form percolated large dislocation loops toward a network of tangled dislocations has been suggested as the origin of this transition[72,73]. Independent TEM studies have demonstrated that at such high ion doses the high density of black dot defects transform into distinguishable large dislocation loops[78]. In addition, the implanted zone loses its elastic response because of the lost constraint between the damaged layer and the irradiated substrate. Instead, with the growth of large dislocation loops, diffuse scattering underneath the Bragg peak becomes strong, as evidenced by X-ray diffuse scattering studies of irradiated Ni, NiCo[90], ZrO_2 [91], UO_2 [35] and MgO [92]. Evidence from recent MD simulations [39] indicate that while the fraction of mono-vacancies, formed in the low fluence regime, decreases in these alloys when the irradiation dose is increased (high

fluence regime), the fraction of larger vacancy clusters increases, which agrees very well with TEM observations during *in situ* [77] or post-irradiation [41] studies.

In order to compare the susceptibility of these alloys to ion-beam induced damage formation at 500 K, selected relative disorder profiles for NiFeCoCr (gree solid line) are depicted in Fig. 9 together with the data for NiFe (blue dash line) and NiCoCr (red dash-dot line) irradiated under identical conditions. Only three ion fluences are shown in Fig. 9: (a) 8, (b) 40, and (c) 80 ions/nm^2. It is obvious that the relative disorder in NiCoCr is always higher compared with NiFe and NiFeCoCr for all indicated fluences. This suggests that NiCoCr exhibits higher susceptibility to ion-beam induced damage formation as compared with NiFe and NiFeCoCr irradiated under identical irradiation conditions. On the other hand, under ion irradiation at 300 K, the irradiation performance of NiCoCr is similar to NiFeCoCr, but better than NiFe, as discussed above and shown in Figs. 2 (a) and 8(a). Decreased mobility of interstitials and formation of large vacancy clusters, which tend to inhibit defect cluster nucleation and growth (e.g., dislocations), has been considered one of the main sources for the improvement of radiation resistance in Ni-based CSAs [36,82,93]. This argument stands true for explaining the irradiation resistance ranking among these alloys (NiCoCr ≈ NiCoFeCr > NiFe) for ion irradiations performed at 300 K, since it has been shown by Granberg et al.[82] that smaller defect clusters are formed in NiCoCr than in NiFe and, more importantly, less likely to grow. In other words, the diffusion coefficients of interstitials in NiCoCr are higher than in NiFe.

One intriguing question is why the response of NiCoCr to ion irradiation is strongly dependent on the irradiation temperature: NiCoCr exhibits higher irradiation resistance than NiFe under ion irradiation at 300 K, while this ranking is inverted under ion irradiations at 500 K. Here it should be mentioned that, while irradiation induced damage at temperatures ≤ 300 K is often controlled by the mobility of interstitials, under ion irradiation at > 300 K (i.e., 500 K) irradiation damage starts to be controlled by the mobility of vacancies, since

conventional thermal diffusion follows the mobility of vacancies. If one assumes that diffusion coefficients of small vacancy clusters in NiFe are higher than in NiCoCr, whereas the diffusion coefficients become lower for large vacancy clusters at high temperature, than we can expect that large clusters can easily migrate and grow to very large sizes in NiCoCr, as revealed by MD snap-shots (see Fig. 7). The high mobility of large vacancy clusters suggests that these clusters can diffuse quickly and coalesce with other clusters emerging into significant levels of cavity swelling. Thus, the diffusion coefficients of vacancies in NiCoCr have to be lower than in NiFe at 500 K to explain the irradiation resistance ranking among these alloys (NiFe > NiCoCr) for ion irradiations performed at 500 K.

Since the densities of NiFe (8.2326 g cm^{-3}) NiCoCr (8.272 g cm^{-3}) and NiCoFeCr (8.144 g cm^{-3}) are similar, the range of injected Ni ions in these samples should be relatively similar. However, the shift of the damage peak in NiCoCr is more pronounced than in NiFe under 1.5 MeV Ni ions at 500 K to a fluence of 80 ions/nm^2 (Fig. 9(c)). In this case, one would therefore expect that any large differences observed in the disorder peak position measured among these alloys under high fluence irradiation must originate from the differences in the defect diffusion kinetics (e.g., vacancy clusters), as discussed previously [36]. This correlation between the vacancy clusters diffusion coefficients and depth shifts in the damage peak position has been successfully applied previously to other CSAs ($Ni_{80}Fe_{20}$ and $Ni_{80}Cr_{20}$), and are generally in good agreement with the extracted depth profile of (defect size) x (defect density) from TEM analysis[34]. These findings underpin the hypothesis that the diffusion coefficients of vacancies as the origin of the temperature-dependent irradiation resistance ranking, and thus provide new insight into previous studies.

4. Summary

Defect accumulation kinetics in FCC NiCoFeCr <100> single crystals irradiated at 500 K have been investigated using Rutherford backscattering spectroscopy in channeling conditions and compared to available literature data for ion-irradiated NiFe and NiCoCr under

identical irradiation conditions (i.e., 1.5 MeV Ni irradiation at 300 and 500 K). In conjunction with independent theoretical calculations and relevant transmission electron microscopy results from literature, unlike previous studies, the underlying mechanism for intriguing temperature-dependent irradiation resistance ranking are discussed. Ion channeling results demonstrate that NiCoCr is not outperforming NiFe anymore under ion irradiation performed in the temperature regimes (i.e., 500 K). At this temperature, vacancies become mobile, influencing defect dynamics and ultimately leading to the aggregation of larger vacancy clusters in NiCoCr than that in NiFe and NiCoFeCr. The origin of this surprisingly temperature-dependent irradiation resistance ranking among these alloys may lie in the energetics of defect migration and its dependence on chemical composition (i.e., lower migration energy of vacancies in NiCoCr, as compared with those in NiFe and NiCoFeCr). In support of this statement, the snapshots of a molecular dynamics cell after a certain number of ion impacts have provided one more piece of evidence: larger defects are observed in NiCoCr than in NiFe, with increasing irradiation temperature. Finally, this review reveals that, to develop CSAs with enhanced radiation resistance, it is imperative to select with extreme caution alloy elements so their vacancy mobility is optimized.

5. Experimental procedures and modeling

Two areas on the <100> orientated equiatomic NiCoFeCr single face-centered cubic (FCC) crystal were irradiated along a non-channeling direction (i.e., NiCoFeCr sample was tilted 7° off the beam axis) at 500 K with 1.5 MeV Ni ions. In these irradiations, the ion fluence ranged from 0.6 to 150 ions/nm^2 to capture the entirety of the defect accumulation process, i.e., the creation of point defects and small clusters up to extended defects, such as SFT. To ensure homogeneity during irradiation, the broad ion beam was slowly rastered over an aperture of 3.0 × 3.0 mm^2 in front of each irradiated area [94,95]. A similar ion flux as in the case of NiCoCr (i.e., ~1.38×10^{-3} /nm^2 /s^1) was used to ensure similar irradiation conditions. In order to monitor the irradiation temperature, the NiCoFeCr sample was mounted onto a

sample holder, which is equipped with a resistive heater and a K-type thermocouple (for details of the experimental setup see Ref. [95]).

After each irradiation step at 500 K, the sample was cooled down to 300 K to minimize thermal annealing effects. Immediately after the sample temperature reached 300 K, the two irradiated areas were analyzed by RBS/C with 3.5 MeV He ions. The backscattered He ions were detected by a Si detector placed at 155° with respect to the incident He beam direction [94]. The depth profile of relative disorder was extracted from the analysis of the RBS/C spectra using an iterative procedure (IP) [96], which has also been applied to analyze CSAs irradiated over a wide range of temperatures (e.g., from 16 K [97] to 500 K [72,73]), revealing good agreement between profiles extracted using this IP are in good agreement with the disorder profiles obtained independently using the RBSADEC (RBS/C of Arbitrary Defected Crystals) [98] and McChasy (Monte Carlo CHAnneling SYmulation)[99] simulation codes. The IP allows the extraction of relative disorder profiles through normalizing the channeling spectra to the random level and subtracting the dechanneling fraction of the analyzing beam. As labeled in Fig. 1(b), the disorder level values can range between 0 (undamaged state) and 1 (amorphous state).

As recently recommended by Weber and Zhang [100], the SRIM code [101] in full-cascade mode has been employed to calculate the depth dependence of atomic displacements, the damage dose (displacements per atom or dpa), and the implanted Ni concentration. The SRIM calculations were performed with the following input values for density and threshold displacement energy for all elements: 8.144 g cm^{-3} and 40 eV [14], respectively. The SRIM predictions show that the most intense collision cascades (i.e., at the damage peak) occur at a depth of about 420 nm.

MD simulations of damage accumulation in single crystalline equiatomic FCC Ni, NiFe and NiCoCr at three different temperatures (300, 500, and 800 K) obtained by previous MD simulations[74] was further analyzed. These simulation results include massively

overlapping cascades conducted under conditions corresponding to the experiments and which have been compared to experiments with good agreement[82,102]. Briefly, thousands of 5 keV collision cascades were introduced in the same simulations cell, reaching a dose of a few tenths of a dpa, which is sufficient to compare to low dose experiments. The cells were homogeneously irradiated and the defect evolution was followed up to the maximum dose. All the simulation details of the study are discussed in Ref.[74]. The simulation cells were analyzed with the Wigner-Seitz analysis[103] to obtain point defect concentrations, and cluster statistics. Defects were considered to belong to the same cluster if their separation distance was less than the midpoint between the second and third nearest neighbor distance. Dislocations were identified with the Dislocation Extraction Algorithm[104] implemented in OVITO[105]. In this article, we re-analyze some of the already reported results in order to better understand the observed experimental results. We mainly focus on the defect cluster size distributions, dislocation densities and types in the damage build-up phase of the simulations, e.g., before saturation, which were not in detail analyzed previously. At very low doses, we observe fewer defects in Ni, and at doses of around 0.1 dpa, we observe a cross-over, where the defect concentration in Ni becomes the highest. In this work, we focus on the regime slightly before, during and after this crossover, to understand what leads to this behavior at different temperatures.

Declaration of Competing Interest

The authors declare that they have no known competing financial interests or personal relationships that could have appeared to influence the work reported in this paper.

Data Availability

The data that support the findings of this study are available from the corresponding authors upon reasonable request.

Acknowledgments

This work was supported as part of the Energy Dissipation to Defect Evolution (EDDE), an Energy Frontier Research Center funded by the US Department of Energy, Office of Science,

Basic Energy Sciences under contract number DE-AC05-00OR22725. The contribution of G. Velişa to this work, after returning to IFIN-HH, was supported under Research Programme Partnership in Priority Areas PNII MEN-UEFISCDI, contract PN 23210201. This work has been partially carried out within the framework of the EUROfusion Consortium, funded by the European Union via the Euratom Research and Training Programme (Grant Agreement No 101052200—EUROfusion). Views and opinions expressed are however those of the author(s) only and do not necessarily reflect those of the European Union or the European Commission. Neither the European Union nor the European Commission can be held responsible for them. Computer time granted by the IT Center for Science—CSC— Finland and the Finnish Grid and Cloud Infrastructure (persistent identifier urn:nbn:fi:research-infras-2016072533) is gratefully acknowledged.

References

1. S. J. Zinkle and G. S. Was: Materials challenges in nuclear energy. *Acta Mater.* **61**(3), 735 (2013).

2. S. J. Zinkle and L. L. Snead: Designing Radiation Resistance in Materials for Fusion Energy. Annu. Rev. Mater. Res. **44**, 241 (2014).

3. M. R. Gilbert, K. Arakawa, Z. Bergstrom, M. J. Caturla, S. L. Dudarev, F. Gao, A. M. Goryaeva, S. Y. Hu, X. Hu, R. J. Kurtz, A. Litnovsky, J. Marian, M. C. Marinica, E. Martinez, E. A. Marquis, D. R. Mason, B. N. Nguyen, P. Olsson, Y. Osetskiy, D. Senor, W. Setyawan, M. P. Short, T. Suzudo, J. R. Trelewicz, T. Tsuru, G. S. Was, B. D. Wirth, L. Yang, Y. Zhang, and S. J. Zinkle: Perspectives on multiscale modelling and experiments to accelerate materials development for fusion. *J. Nucl. Mater.* **554**, 153113 (2021).

4. Y. Zhang, L. Wang, and W. J. Weber: Charged particles: Unique tools to study irradiation resistance of concentrated solid solution alloys. *J. Mater. Sci. Technol.* **140**, 260 (2023).

5. B. Cantor, I. T. H. Chang, P. Knight, and A. J. B. Vincent: Microstructural development in equiatomic multicomponent alloys. *Mater. Sci. Eng. A* **375**–**377**, 213 (2004).

6. J. W. Yeh, S. K. Chen, S. J. Lin, J. Y. Gan, T. S. Chin, T. T. Shun, C. H. Tsau, and S. Y. Chang: Nanostructured High-Entropy Alloys with Multiple Principal Elements: Novel Alloy Design Concepts and Outcomes. *Adv. Eng. Mater.* **6**(5), 299 (2004).

7. B. Gludovatz, A. Hohenwarter, K. V. S. Thurston, H. Bei, Z. Wu, E. P. George, and R. O. Ritchie: Exceptional damage-tolerance of a medium-entropy alloy CrCoNi at cryogenic temperatures. *Nat. Commun.* **7**(1), 10602 (2016).

8. E. P. George, D. Raabe, and R. O. Ritchie: *Nat. Rev. Mater.* **4**, 515 (2019).

9. Z. Wu, H. Bei, G. M. Pharr, and E. P. George: Temperature dependence of the mechanical properties of equiatomic solid solution alloys with face-centered cubic crystal structures. *Acta Mater.* **81**, 428 (2014).

10. Y. Shi, B. Yang, and P. K. Liaw: Corrosion-Resistant High-Entropy Alloys: A Review. *Met.* 7(2) 43 (2017).

11. B. Gludovatz, A. Hohenwarter, D. Catoor, E. H. Chang, E. P. George, and R. O. Ritchie: A fracture-resistant high-entropy alloy for cryogenic applications. *Science*

345(6201), 1153 (2014).

12. M.-H. Tsai and J.-W. Yeh: High-Entropy Alloys: A Critical Review. *Mater. Res. Lett.* **2**(3), 107 (2014).

13. D. B. B. Miracle and O. N. N. Senkov: A critical review of high entropy alloys and related concepts. *Acta Mater.* **122**, 448 (2017).

14. Y. Zhang, G. M. Stocks, K. Jin, C. Lu, H. Bei, B. C. Sales, L. Wang, L. K. Béland, R. E. Stoller, G. D. Samolyuk, M. Caro, A. Caro, and W. J. Weber: Influence of chemical disorder on energy dissipation and defect evolution in concentrated solid solution alloys. *Nat. Commun.* **6**(1), 8736 (2015).

15. Y. Zhang, T. Egami, and W. J. Weber: Dissipation of radiation energy in concentrated solid-solution alloys: Unique defect properties and microstructural evolution. *MRS Bull.* **44**(10), 798 (2019).

16. E. J. Pickering, A. W. Carruthers, P. J. Barron, S. C. Middleburgh, D. E. J. Armstrong, and A. S. Gandy: High-Entropy Alloys for Advanced Nuclear Applications. *Entropy* **23**(1), 98 (2021).

17. Z. Zhang, D. E. J. Armstrong, and P. S. Grant: The effects of irradiation on CrMnFeCoNi high-entropy alloy and its derivatives. *Prog. Mater. Sci.* **123**, 100807 (2022).

18. Y. Zhang, Y. N. Osetsky, and W. J. Weber: Tunable Chemical Disorder in Concentrated Alloys: Defect Physics and Radiation Performance. *Chem. Rev.* **122**(1), 789 (2022).

19. Y. Zhang, C. Silva, T. G. Lach, M. A. Tunes, Y. Zhou, L. Nuckols, W. L. Boldman, P. D. Rack, S. E. Donnelly, L. Jiang, L. Wang, and W. J. Weber: Role of electronic energy loss on defect production and interface stability: Comparison between ceramic materials and high-entropy alloys. *Curr. Opin. Solid State Mater. Sci.* **26**(4), 101001 (2022).

20. M. Moschetti, P. Burr, E. Obbard, J. J. Kruzic, P. Hosemann, and B. Gludovatz: Design considerations for high entropy alloys in advanced nuclear applications. *J. Nucl. Mater.* 153814 (2022).

21. Y. Zhang and W. J. Weber: Ion irradiation and modification: The role of coupled electronic and nuclear energy dissipation and subsequent nonequilibrium processes in materials. *Appl. Phys. Rev.* **7**(4), 041307 (2020).

22. Y. Zhang: Reassembled nanoprecipitates resisting radiation. *Nat. Mater.* (2022).

23. B. Cantor: Multicomponent and High Entropy Alloys. *Entropy 2014, Vol. 16, Pages 4749-4768* **16**(9), 4749 (2014).

24. Y. Zhang, K. Jin, H. Xue, C. Lu, R. J. Olsen, L. K. Beland, M. W. Ullah, S. Zhao, H. Bei, D. S. Aidhy, G. D. Samolyuk, L. Wang, M. Caro, A. Caro, G. M. Stocks, B. C. Larson, I. M. Robertson, A. A. Correa, and W. J. Weber: Influence of chemical disorder on energy dissipation and defect evolution in advanced alloys. *J. Mater. Res.* **31**(16), 2363 (2016).

25. Y. Zhang, S. Zhao, W. J. Weber, K. Nordlund, F. Granberg, and F. Djurabekova: Atomic-level heterogeneity and defect dynamics in concentrated solid-solution alloys.

Curr. Opin. Solid State Mater. Sci. **21**(5), 221 (2017).

26. R. Zhang, S. Zhao, J. Ding, Y. Chong, T. Jia, C. Ophus, M. Asta, R. O. Ritchie, and A. M. Minor: Short-range order and its impact on the CrCoNi medium-entropy alloy. *Nature* **581**(7808), 283 (2020).

27. S. Mu, Z. Pei, X. Liu, and G. M. Stocks: Electronic transport and phonon properties of maximally disordered alloys: From binaries to high-entropy alloys. *J. Mater. Res.* **33**(19), 2857 (2018).

28. W. R. Jian, Z. Xie, S. Xu, Y. Su, X. Yao, and I. J. Beyerlein: Effects of lattice distortion and chemical short-range order on the mechanisms of deformation in medium entropy alloy CoCrNi. *Acta Mater.* **199**, 352 (2020).

29. E. Lu, J. Zhao, I. Makkonen, K. Mizohata, Z. Li, M. Hua, F. Djurabekova, and F. Tuomisto: Enhancement of vacancy diffusion by C and N interstitials in the equiatomic FeMnNiCoCr high entropy alloy. *Acta Mater.* **215**, 117093 (2021).

30. E. Wendler, O. Bilani, K. Gärtner, W. Wesch, M. Hayes, F. D. Auret, K. Lorenz, and E. Alves: Radiation damage in ZnO ion implanted at 15 K. *Nucl. Instrum. Meth. Phys. Res. Sect. B* **267**(16), 2708 (2009).

31. Y. Haddad, L. Delauche, A. Gentils, and F. Garrido: In situ characterization of irradiation-induced microstructural evolution in urania single crystals at 773 K. *Nucl. Instrum. Meth. Phys. Res. Sect. B* **435**, 25 (2018).

32. K. Yasuda, M. Nastasi, K. E. Sickafus, C. J. Maggiore, and N. Yu: Ion beam channeling study on the damage accumulation in yttria-stabilized cubic zirconia. *Nucl. Instrum. Meth. Phys. Res. Sect. B* **136**–**138**, 499 (1998).

33. A. Turos, P. Jóźwik, M. Wójcik, J. Gaca, R. Ratajczak, and A. Stonert: Mechanism of damage buildup in ion bombarded ZnO. *Acta Mater.* **134**, 249 (2017).

34. K. Jin, G. Velisa, H. Xue, T. Yang, H. Bei, W. J. Weber, L. Wang, and Y. Zhang: Channeling analysis in studying ion irradiation damage in materials containing various types of defects. *J. Nucl. Mater.* **517**, 9 (2019).

35. X. Jin, A. Boulle, A. Chartier, J. P. Crocombette, and A. Debelle: Analysis of strain and disordering kinetics based on combined RBS-channeling and X-ray diffraction atomic-scale modelling. *Acta Mater.* **201**, 63 (2020).

36. S. Zhao, G. Velisa, H. Xue, H. Bei, W. J. Weber, and Y. Zhang: Suppression of vacancy cluster growth in concentrated solid solution alloys. *Acta Mater.* **125**, 231 (2017).

37. M. R. He, S. Wang, S. Shi, K. Jin, H. Bei, K. Yasuda, S. Matsumura, K. Higashida, and I. M. Robertson: Mechanisms of radiation-induced segregation in CrFeCoNi-based single-phase concentrated solid solution alloys. *Acta Mater.* **126**, 182 (2017).

38. C. Lu, T. Yang, K. Jin, N. Gao, P. Xiu, Y. Zhang, F. Gao, H. Bei, W. J. Weber, K. Sun, Y. Dong, and L. Wang: Radiation-induced segregation on defect clusters in single-phase concentrated solid-solution alloys. *Acta Mater.* **127**, 98 (2017).

39. F. Tuomisto, I. Makkonen, J. Heikinheimo, F. Granberg, F. Djurabekova, K. Nordlund, G. Velisa, H. Bei, H. Xue, W. J. Weber, and Y. Zhang: Segregation of Ni at early stages of radiation damage in NiCoFeCr solid solution alloys. *Acta Mater.* **196**, 44

(2020).

40. K. Jin, C. Lu, L. M. Wang, J. Qu, W. J. Weber, Y. Zhang, and H. Bei: Effects of compositional complexity on the ion-irradiation induced swelling and hardening in Ni-containing equiatomic alloys. *Scr. Mater.* **119**(July), 65 (2016).

41. C. Lu, L. Niu, N. Chen, K. Jin, T. Yang, P. Xiu, Y. Zhang, F. Gao, H. Bei, S. Shi, M. R. He, I. M. Robertson, W. J. Weber, and L. Wang: Enhancing radiation tolerance by controlling defect mobility and migration pathways in multicomponent single-phase alloys. *Nat. Commun.* **7**, 1 (2016).

42. T. Yang, C. Lu, K. Jin, M. L. Crespillo, Y. Zhang, H. Bei, and L. Wang: The effect of injected interstitials on void formation in self-ion irradiated nickel containing concentrated solid solution alloys. *J. Nucl. Mater.* **488**, 328 (2017).

43. Y. Zhang, X. Wang, Y. N. Osetsky, Y. Tong, R. Harrison, S. E. Donnelly, D. Chen, Y. Wang, H. Bei, B. C. Sales, K. L. More, P. Xiu, L. Wang, and W. J. Weber: Effects of 3d Electron Configurations on Helium Bubble Formation and Void Swelling in Concentrated Solid-Solution Alloys. **181** 519-529 (2019).

44. Y. N. Osetsky, L. K. Béland, A. V. Barashev, and Y. Zhang: On the existence and origin of sluggish diffusion in chemically disordered concentrated alloys. *Curr. Opin. Solid State Mater. Sci.* **22**(3), 65 (2018).

45. A. Barashev, Y. Osetsky, H. Bei, C. Lu, L. Wang, and Y. Zhang: Chemically-biased diffusion and segregation impede void growth in irradiated Ni-Fe alloys. *Curr. Opin. Solid State Mater. Sci.* **23**(2), 92 (2019).

46. Q. Fang, J. Peng, Y. Chen, L. Li, H. Feng, J. Li, C. Jiang, and P. K. Liaw: Hardening behaviour in the irradiated high entropy alloy. *Mech. Mater.* **155**, 103744 (2021).

47. S. Q. Xia, X. Yang, T. F. Yang, S. Liu, and Y. Zhang: Irradiation Resistance in AlxCoCrFeNi High Entropy Alloys. *JOM* **67**(10), 2340 (2015).

48. S. Chang, K. K. Tseng, T. Y. Yang, D. S. Chao, J. W. Yeh, and J. H. Liang: Irradiation-induced swelling and hardening in HfNbTaTiZr refractory high-entropy alloy. *Mater. Lett.* **272**, 127832 (2020).

49. N. A. P. K. Kumar, C. Li, K. J. Leonard, H. Bei, and S. J. Zinkle: Microstructural stability and mechanical behavior of FeNiMnCr high entropy alloy under ion irradiation. *Acta Mater.* **113**, 230 (2016).

50. E. Lu, I. Makkonen, K. Mizohata, Z. Li, J. Räisänen, and F. Tuomisto: Effect of interstitial carbon on the evolution of early-stage irradiation damage in equi-atomic FeMnNiCoCr high-entropy alloys. *J. Appl. Phys.* **127**(2), 025103 (2020).

51. M. A. Cusentino, M. A. Wood, and R. Dingreville: Compositional and structural origins of radiation damage mitigation in high-entropy alloys. *J. Appl. Phys.* **128**(12), 125904 (2020).

52. W. Y. Chen, J. D. Poplawsky, Y. Chen, W. Guo, and J. W. Yeh: Irradiation-induced segregation at dislocation loops in CoCrFeMnNi high entropy alloy. *Materialia* **14**, 100951 (2020).

53. P. P. Cao, H. Wang, J. Y. He, C. Xu, S. H. Jiang, J. L. Du, X. Z. Cao, E. G. Fu, and Z. P. Lu: Effects of nanosized precipitates on irradiation behavior of CoCrFeNi high

entropy alloys. *J. Alloys Compd.* **859**, 158291 (2021).

54. J. Kim, J. W. Lim, J. K. Kim, D. H. Kim, E. S. Park, and H. J. Chang: Suppressed radiation-induced dynamic recrystallization in CrFeCoNiCu high-entropy alloy. *Scr. Mater.* **190**, 158 (2021).

55. M. Aizenshtein, Z. Ungarish, K. B. B. Woller, S. Hayun, and M. P. P. Short: Mechanical and microstructural response of the Al0.5CoCrFeNi high entropy alloy to Si and Ni ion irradiation. *Nucl. Mater. Energy* **25**, 100813 (2020).

56. Y. Lin, T. Yang, L. Lang, C. Shan, H. Deng, W. Hu, and F. Gao: Enhanced radiation tolerance of the Ni-Co-Cr-Fe high-entropy alloy as revealed from primary damage. *Acta Mater.* **196**, 133 (2020).

57. X. X. Wang, L. L. Niu, and S. Wang: Interpreting radiation-induced segregation and enhanced radiation tolerance of single-phase concentrated solid-solution alloys from first principles. *Mater. Lett.* **202**, 120 (2017).

58. Y. Li, R. Li, Q. Peng, and S. Ogata: Reduction of dislocation, mean free path, and migration barriers using high entropy alloy: Insights from the atomistic study of irradiation damage of CoNiCrFeMn. *Nanotechnology* **31**(42), 8 (2020).

59. S. C. Middleburgh, D. M. King, G. R. Lumpkin, M. Cortie, and L. Edwards: Segregation and migration of species in the CrCoFeNi high entropy alloy. *J. Alloys Compd.* **599**, 179 (2014).

60. T. Yang, S. Xia, W. Guo, R. Hu, J. D. Poplawsky, G. Sha, Y. Fang, Z. Yan, C. Wang, C. Li, Y. Zhang, S. J. Zinkle, and Y. Wang: Effects of temperature on the irradiation responses of Al0.1CoCrFeNi high entropy alloy. *Scr. Mater.* **144**, 31 (2018).

61. S. Xia, M. C. Gao, T. Yang, P. K. Liaw, and Y. Zhang: Phase stability and microstructures of high entropy alloys ion irradiated to high doses. *J. Nucl. Mater.* **480**, 100 (2016).

62. C. M. Barr, J. E. Nathaniel, K. A. Unocic, J. Liu, Y. Zhang, Y. Wang, and M. L. Taheri: Exploring radiation induced segregation mechanisms at grain boundaries in equiatomic CoCrFeNiMn high entropy alloy under heavy ion irradiation. *Scr. Mater.* **156**, 80 (2018).

63. C. Lu, T. Yang, K. Jin, G. Velisa, P. Xiu, M. Song, Q. Peng, F. Gao, Y. Zhang, H. Bei, W. J. Weber, and L. Wang: Enhanced void swelling in NiCoFeCrPd high-entropy alloy by indentation-induced dislocations. *Mater. Res. Lett.* **6**(10), 584 (2018).

64. T. Yang, W. Guo, J. D. Poplawsky, D. Li, L. Wang, Y. Li, W. Hu, M. L. Crespillo, Z. Yan, Y. Zhang, Y. Wang, and S. J. Zinkle: Structural damage and phase stability of Al0.3CoCrFeNi high entropy alloy under high temperature ion irradiation. *Acta Mater.* **188**, 1 (2020).

65. W. Y. Chen, M. A. Kirk, N. Hashimoto, J. W. Yeh, X. Liu, and Y. Chen: Irradiation effects on Al0.3CoCrFeNi and CoCrMnFeNi high-entropy alloys, and 316H stainless steel at 500 °C. *J. Nucl. Mater.* **539**, 152324 (2020).

66. X. Wang, C. Hatzoglou, B. Sneed, Z. Fan, W. Guo, K. Jin, D. Chen, H. Bei, Y. Wang, W. J. Weber, Y. Zhang, B. Gault, K. L. More, F. Vurpillot, and J. D. Poplawsky: Interpreting nanovoids in atom probe tomography data for accurate local compositional

measurements. *Nat. Commun.* **11**(1), 1 (2020).

67. S. Abhaya, R. Rajaraman, R. M. Sarguna, P. K. Parida, C. David, and G. Amarendra: Defect microstructure in high temperature Ni+ implanted FeCrCoNi-a positron beam study. *J. Alloys Compd.* **806**, 780 (2019).

68. S. Abhaya, R. Rajaraman, S. Kalavathi, C. David, B. K. Panigrahi, and G. Amarendra: Effect of dose and post irradiation annealing in Ni implanted high entropy alloy FeCrCoNi using slow positron beam. *J. Alloys Compd.* **669**, 117 (2016).

69. T. R. Allen, J. T. Busby, G. S. Was, and E. A. Kenik: On the mechanism of radiation-induced segregation in austenitic Fe-Cr-Ni alloys. *J. Nucl. Mater.* **255**(1), 44 (1998).

70. T. Takeyama, H. Takahashi, and, S. Ohnuki: Radiation-Induced Segregation in Austenitic and Ferritic Steels. *Bulletin of the Faculty of Engineering. Hokkaido University*. **121** 85-99 (1984).

71. M. Vaidya, K. G. Pradeep, B. S. Murty, G. Wilde, and S. V. Divinski: Bulk tracer diffusion in CoCrFeNi and CoCrFeMnNi high entropy alloys. *Acta Mater.* **146**, 211 (2018).

72. G. Velişa, Z. Fan, M. L. Crespillo, H. Bei, W. J. Weber, and Y. Zhang: Temperature effects on damage evolution in ion-irradiated NiCoCr concentrated solid-solution alloy. *J. Alloys Compd.* **832**, 154918 (2020).

73. Z. Fan, G. Velisa, K. Jin, M. L. Crespillo, H. Bei, W. J. Weber, and Y. Zhang: Temperature-dependent defect accumulation and evolution in Ni-irradiated NiFe concentrated solid-solution alloy. *J. Nucl. Mater.* **519**, 1 (2019).

74. E. Levo, F. Granberg, K. Nordlund, and F. Djurabekova: Temperature effect on irradiation damage in equiatomic multi-component alloys. *Comput. Mater. Sci.* **197**, 110571 (2021).

75. G. Velişa, K. Jin, Z. Fan, C. Lu, H. Bei, W. J. Weber, L. Wang, and Y. Zhang: Multi-axial and multi-energy channeling study of disorder evolution in ion-irradiated nickel. *J. Nucl. Mater.* **525**, 92 (2019).

76. Y. Zhou, G. Velişa, S. San, M. L. Crespillo, Z. Fan, H. Bei, W. J. Weber, P. Xiu, L. Wang, F. Tuomisto, W.-Y. Ching, and Y. Zhang: Role of chemical disorder on radiation-induced defect production and damage evolution in NiFeCoCr. *J. Nucl. Mater.* **565**, 153689 (2022).

77. S. Shi, M.-R. He, K. Jin, H. Bei, and I. M. Robertson: Evolution of ion damage at 773K in Ni- containing concentrated solid-solution alloys. *J. Nucl. Mater.* **501**, 132 (2018).

78. C. Lu, K. Jin, L. K. Béland, F. Zhang, T. Yang, L. Qiao, Y. Zhang, H. Bei, H. M. Christen, R. E. Stoller, and L. Wang: Direct Observation of Defect Range and Evolution in Ion-Irradiated Single Crystalline Ni and Ni Binary Alloys. *Sci. Rep.* **6**(1), 19994 (2016).

79. W. Wesch and E. Wendler: Ion Beam Modification of Solids : Ion-Solid Interaction and Radiation Damage (2016).

80. F. Tuomisto and I. Makkonen: Defect identification in semiconductors with positron annihilation: Experiment and theory. *Rev. Mod. Phys.* **85**(4), 1583 (2013).

81. K. Jin, B. C. Sales, G. M. Stocks, G. D. Samolyuk, M. Daene, W. J. Weber, Y. Zhang, and H. Bei: Tailoring the physical properties of Ni-based single-phase equiatomic alloys by modifying the chemical complexity. *Sci. Rep.* **6** (2016).

82. F. Granberg, K. Nordlund, M. W. Ullah, K. Jin, C. Lu, H. Bei, L. M. Wang, F. Djurabekova, W. J. Weber, and Y. Zhang: Mechanism of Radiation Damage Reduction in Equiatomic Multicomponent Single Phase Alloys. *Phys. Rev. Lett.* **116**(13), 135504 (2016).

83. E. Levo, F. Granberg, C. Fridlund, K. Nordlund, and F. Djurabekova: Radiation damage buildup and dislocation evolution in Ni and equiatomic multicomponent Ni-based alloys. *J. Nucl. Mater.* **490**, 323 (2017).

84. F. Granberg, F. Djurabekova, E. Levo, and K. Nordlund: Damage buildup and edge dislocation mobility in equiatomic multicomponent alloys. *Nucl. Instrum. Meth. Phys. Res. Sect. B* **393**, 114 (2017).

85. M. W. Ullah, Y. Zhang, N. Sellami, A. Debelle, H. Bei, and W. J. Weber: Evolution of irradiation-induced strain in an equiatomic NiFe alloy. *Scr. Mater.* **140**, 35 (2017).

86. D. S. Aidhy, C. Lu, K. Jin, H. Bei, Y. Zhang, L. Wang, and W. J. Weber: Point defect evolution in Ni, NiFe and NiCr alloys from atomistic simulations and irradiation experiments. *Acta Mater.* **99**, 69 (2015).

87. D. S. Aidhy, P. C. Millett, T. Desai, D. Wolf, and S. R. Phillpot: Kinetically evolving irradiation-induced point defect clusters in UO 2 by molecular dynamics simulation. *Phys. Rev. B* **80**, 104107 (2009).

88. D. S. Aidhy, P. C. Millett, D. Wolf, S. R. Phillpot, and H. Huang: Kinetically driven point-defect clustering in irradiated MgO by molecular-dynamics simulation. *Scr. Mater.* **60**(8), 691 (2009).

89. S. Abhaya, R. Rajaraman, S. Kalavathi, and G. Amarendra: Positron annihilation studies on FeCrCoNi high entropy alloy. *J. Alloys Compd.* **620**, 277 (2015).

90. R. J. Olsen, K. Jin, C. Lu, L. K. Beland, L. Wang, H. Bei, E. D. Specht, and B. C. Larson: Investigation of defect clusters in ion-irradiated Ni and NiCo using diffuse X-ray scattering and electron microscopy. *J. Nucl. Mater.* **469**, 153 (2016).

91. S. Moll, L. Thomé, G. Sattonnay, A. Debelle, F. Garrido, L. Vincent, and J. Jagielski: Multistep damage evolution process in cubic zirconia irradiated with MeV ions. *J. Appl. Phys.* **106**(7), 073509 (2009).

92. S. Moll, Y. Zhang, A. Debelle, L. Thomé, J. P. Crocombette, Z. Zihua, J. Jagielski, and W. J. Weber: Damage processes in MgO irradiated with medium-energy heavy ions. *Acta Mater.* **88**, 314 (2015).

93. S. Zhao, Y. Osetsky, and Y. Zhang: Preferential diffusion in concentrated solid solution alloys: NiFe, NiCo and NiCoCr. *Acta Mater.* **128**, 391 (2017).

94. Y. Zhang, M. L. Crespillo, H. Xue, K. Jin, C. H. Chen, C. L. Fontana, J. T. Graham, and W. J. Weber: New ion beam materials laboratory for materials modification and irradiation effects research. N*ucl. Instrum. Meth. Phys. Res. Sect. B* **338**, 19 (2014).

95. M. L. Crespillo, J. T. Graham, Y. Zhang, and W. J. Weber: Temperature measurements during high flux ion beam irradiations. *Rev. Sci. Instrum.* **87**(2), 024902 (2016).

96. Y. Zhang, J. Lian, Z. Zhu, W. D. Bennett, L. V. Saraf, J. L. Rausch, C. A. Hendricks, R. C. Ewing, and W. J. Weber: Response of strontium titanate to ion and electron irradiation. *J. Nucl. Mater.* **389**(2), 303 (2009).

97. G. Velişa, E. Wendler, S. Zhao, K. Jin, H. Bei, W. J. Weber, and Y. Zhang: Delayed damage accumulation by athermal suppression of defect production in concentrated solid solution alloys. *Mater. Res. Lett.* **6**(2), 136 (2018).

98. S. Zhang, K. Nordlund, F. Djurabekova, Y. Zhang, G. Velisa, and T. S. Wang: Simulation of Rutherford backscattering spectrometry from arbitrary atom structures. *Phys. Rev. E* **94**(4), 1 (2016).

99. C. Mieszczynski, R. Ratajczak, J. Jagielski, G. Velişa, H. Bei, B. C. Sales, E. Wendler, W. J. Weber, and Y. Zhang: Defect evolution in Ni and solid-solution alloys of NiFe and NiFeCoCr under ion irradiation at 16 and 300 K. *J. Nucl. Mater.* **534**, 152138 (2020).

100. W. J. Weber and Y. Zhang: Predicting damage production in monoatomic and multi-elemental targets using stopping and range of ions in matter code: Challenges and recommendations. *Curr. Opin. Solid State Mater. Sci.* **23**(4), 100757 (2019).

101. J. F. Ziegler and J. P. Biersack: in *Treatise Heavy-Ion Sci.* (Springer US, Boston, MA, 1985), pp. 93–129.

102. S. Zhang, K. Nordlund, F. Djurabekova, F. Granberg, Y. Zhang, and T. S. Wang: Radiation damage buildup by athermal defect reactions in nickel and concentrated nickel alloys. *Mater. Res. Lett.* **5**(6), 433-439 (2017).

103. K. Nordlund, M. Ghaly, R. S. Averback, M. Caturla, T. D. de la Rubia, and J. Tarus: Defect production in collision cascades in elemental semiconductors and fcc metals. *Phys. Rev. B* **57**(13), 7556 (1998).

104. A. Stukowski: Visualization and analysis of atomistic simulation data with OVITO–the Open Visualization Tool. *Model. Simul. Mater. Sci. Eng.* **18**(1), 015012 (2009).

105. A. Stukowski, V. V. Bulatov, and A. Arsenlis: Automated identification and indexing of dislocations in crystal interfaces. *Model. Simul. Mater. Sci. Eng.* **20**(8), 085007 (2012).

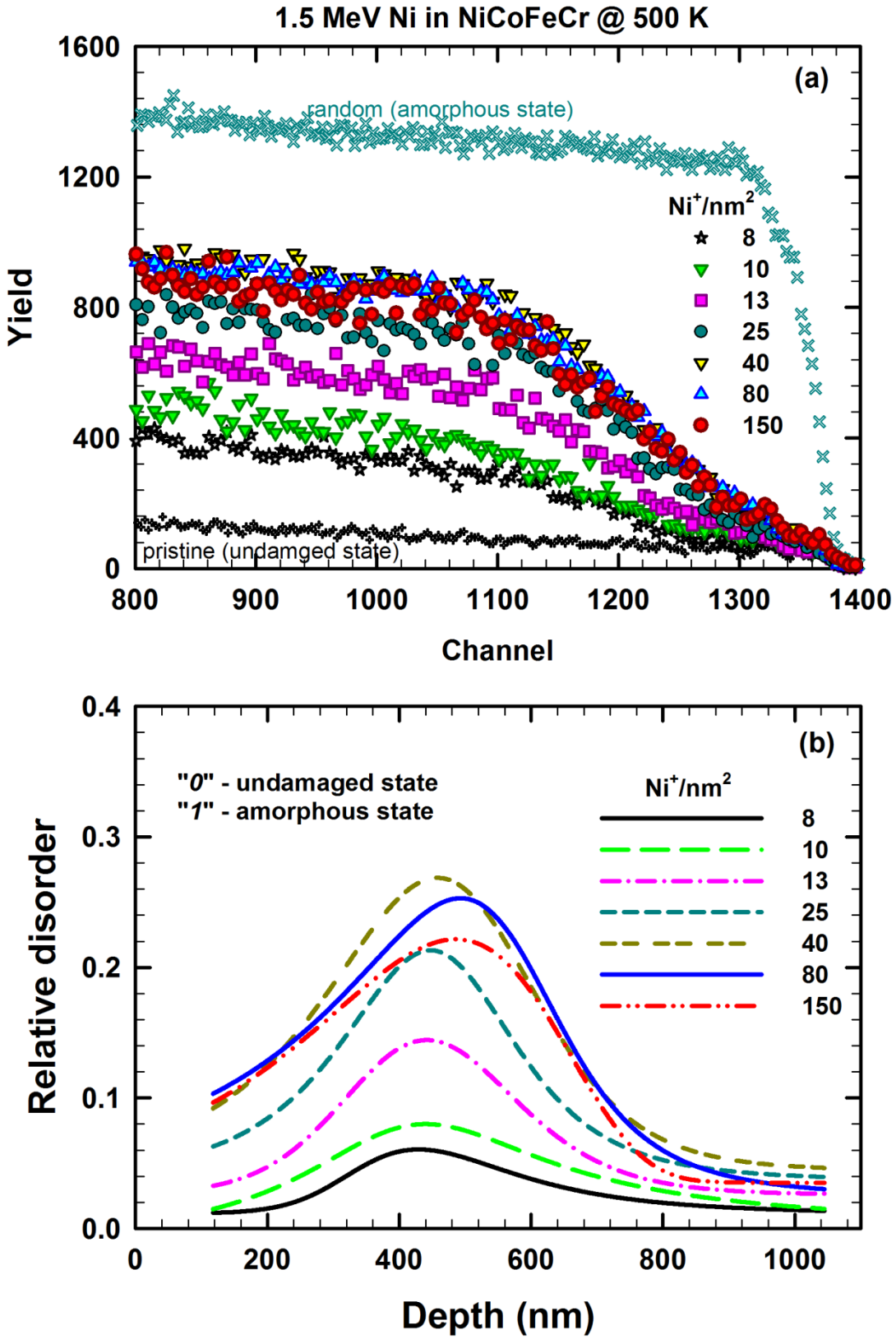

Fig. 1: (a) Typical RBS/C spectra recorded from NiCoFeCr irradiated with 1.5 MeV Ni^+ ions at 500 K. The ion fluences are indicated in the legend. (b) Disorder profiles obtained from the analysis RBS/C spectra (a) by applying the iterative procedure. For visual clarity, only the best fits to experimental data are depicted in Fig. 1(b).

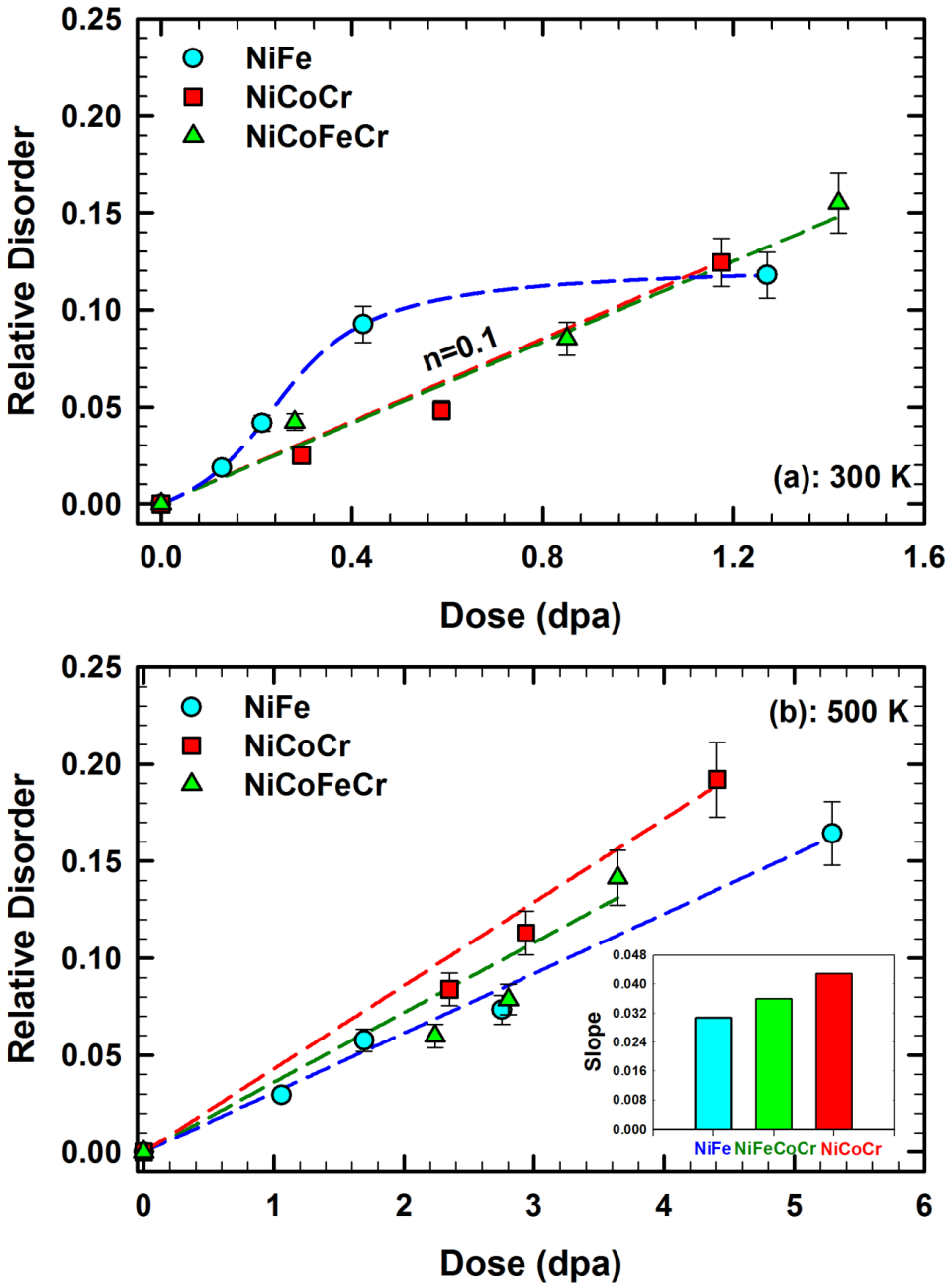

Fig. 2: Comparison of the early stages damage evolution observed by RBS/C in NiFe [73] (blue filled circles), NiCoCr [72] (red filled squares) and NiCoFeCr [76] (green filled triangles) irradiated with 1.5 MeV Ni ions at: (a) 300 K and (b) 500 K. The results for NiCoCr irradiated under similar irradiation conditions are taken from Ref. [72]. The lines are curve fits to guide the eye. The slope dependence on alloy composition obtained from fits are shown in the inset. Note that the slope unity is relative disorder/dpa.

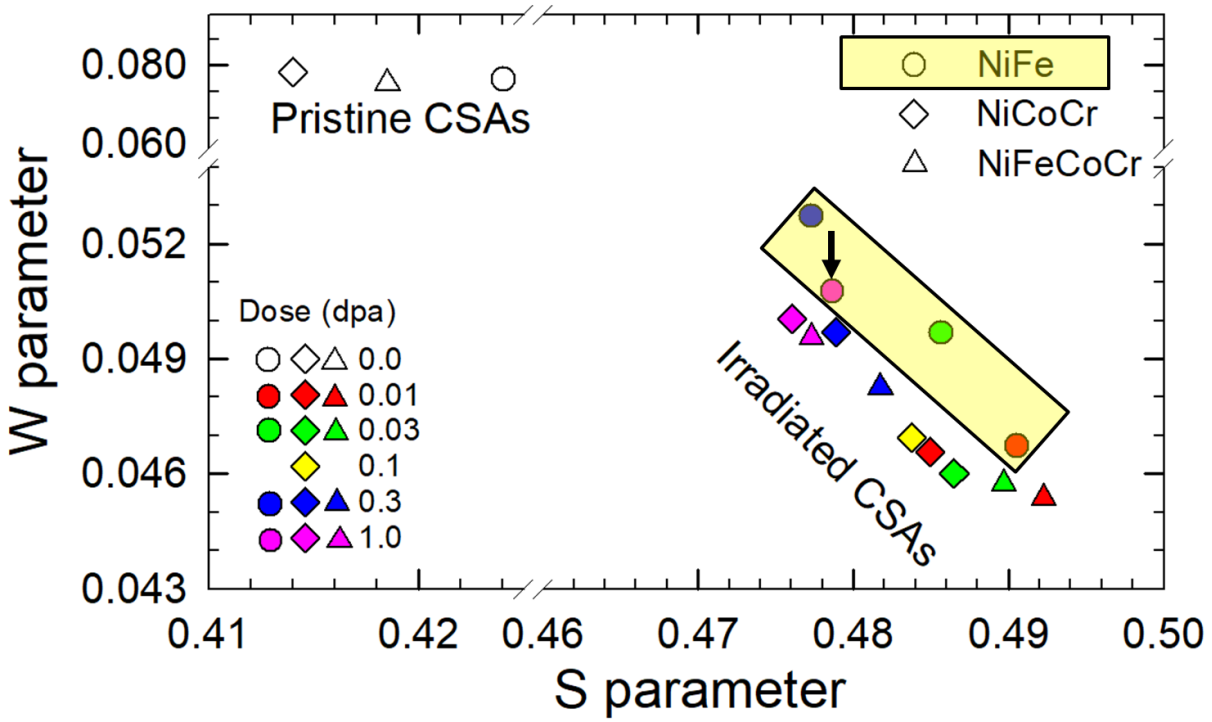

Fig. 3: Dose dependence of the (S, W) parameters for NiFe, NiCoCr and NiCoFeCr irradiated at 300 K using Ni ions with multiple energies (2, 4, 8 and 16 MeV) at various ion doses (ranging from 0.01 to 1 dpa). The S-W data sets for pristine (unirradiated) samples are included for comparison. In order to clearly point out the region where the data sets of irradiated NiFe are situated, we have covered them with a transparent rectangle.

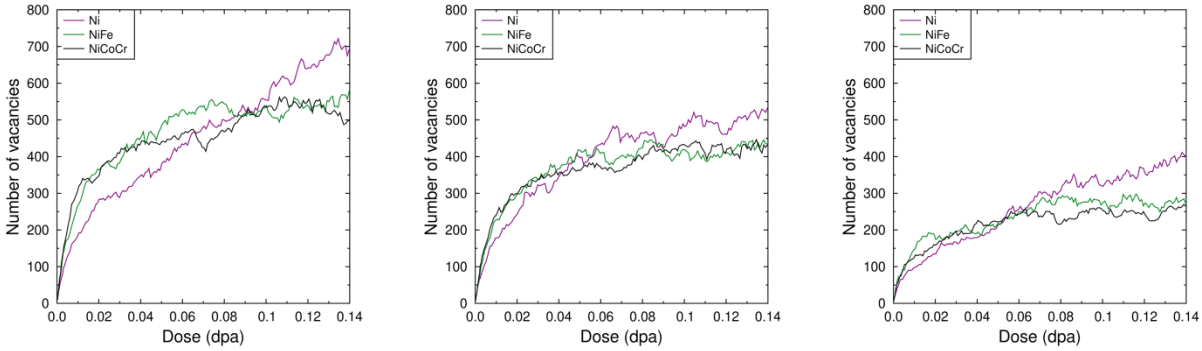

(a) 300K (b) 500K (c) 800K

Fig. 4: Number of vacancies (FPs) as a function of dose at: (a) 300, (b) 500, and (c) 800K.

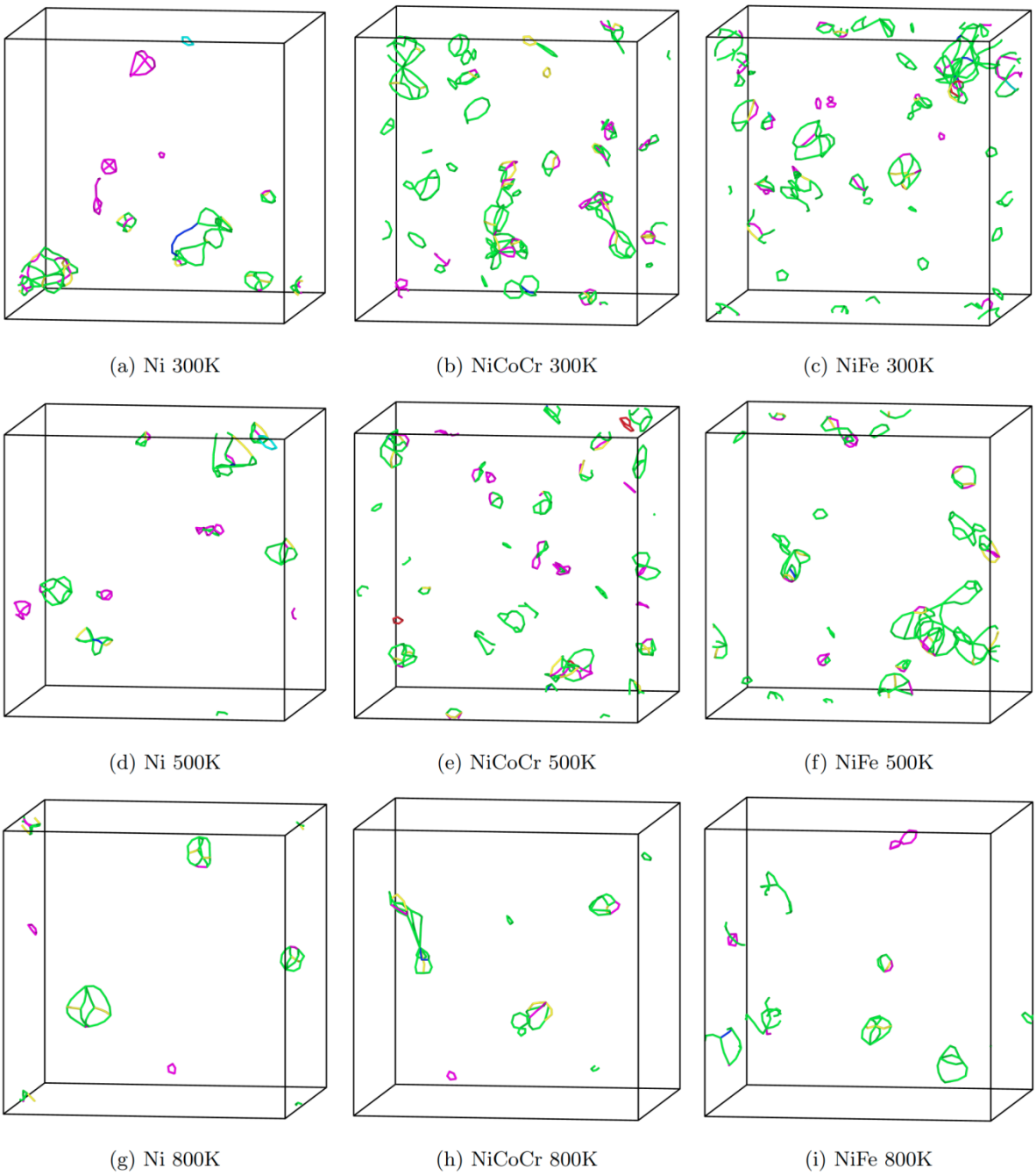

Fig. 5: Comparison of the dislocation evolution observed by MD in Ni (left column), NiCoCr (middle column) and NiFe (right column), before the crossover, for all three temperatures.

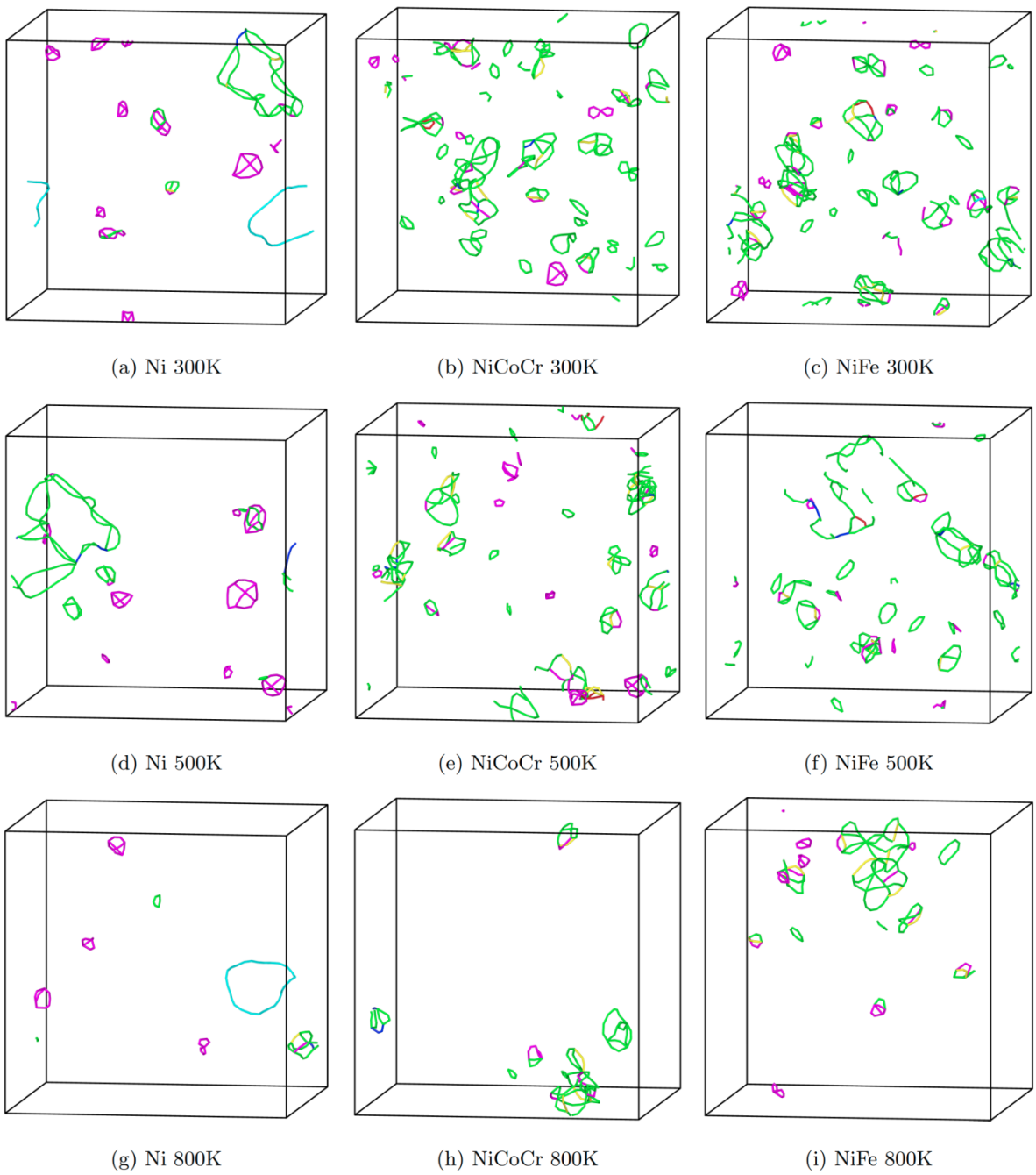

Fig. 6: Comparison of the dislocation evolution observed by MD in Ni (left column), NiCoCr (middle column) and NiFe (right column), at the crossover, for all three temperatures.

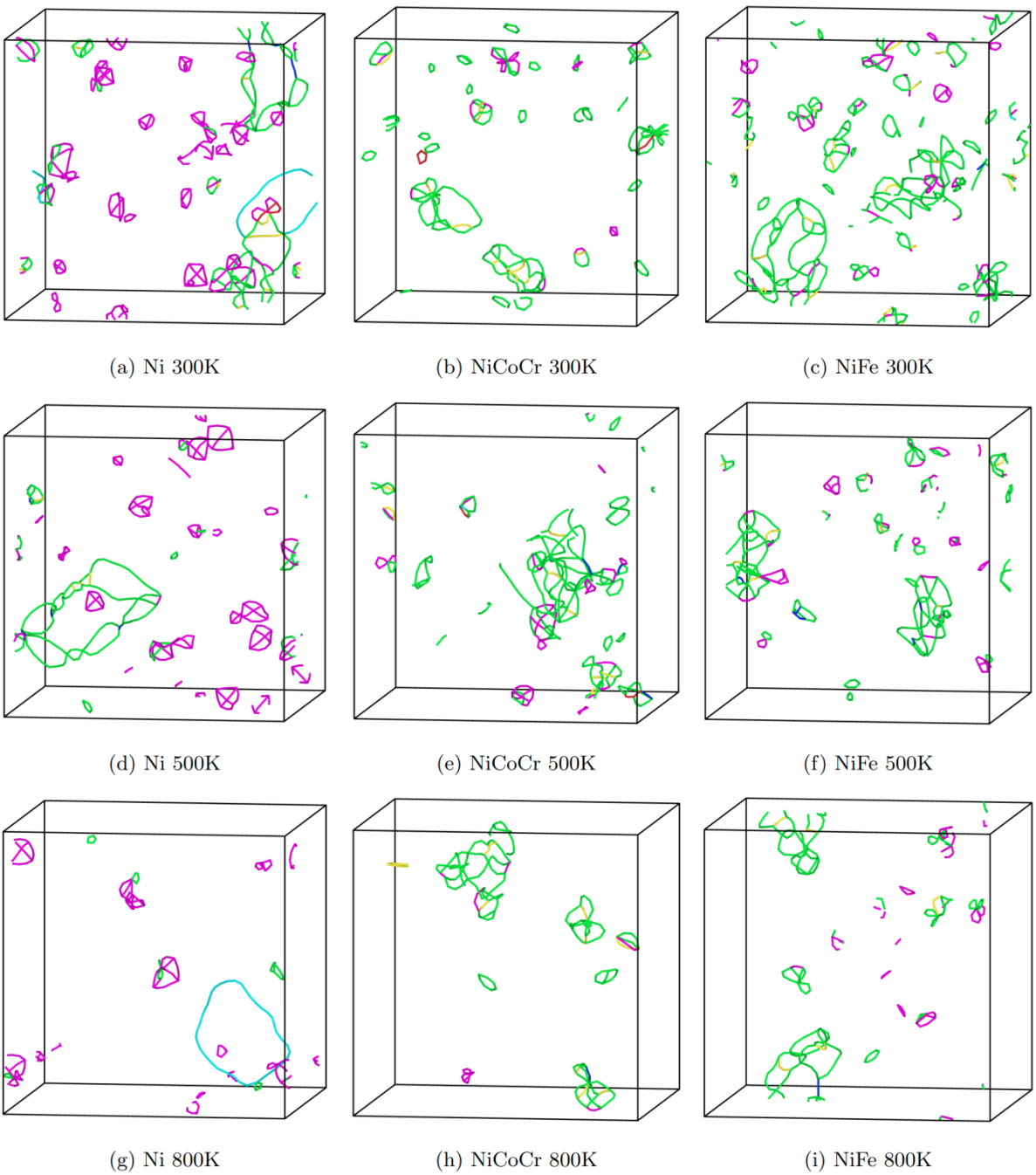

(a) Ni 300K (b) NiCoCr 300K (c) NiFe 300K

(d) Ni 500K (e) NiCoCr 500K (f) NiFe 500K

(g) Ni 800K (h) NiCoCr 800K (i) NiFe 800K

Fig. 7: Comparison of the dislocation evolution observed by MD in Ni (left column), NiCoCr (middle column) and NiFe (right column), after the crossover, for all three temperatures.

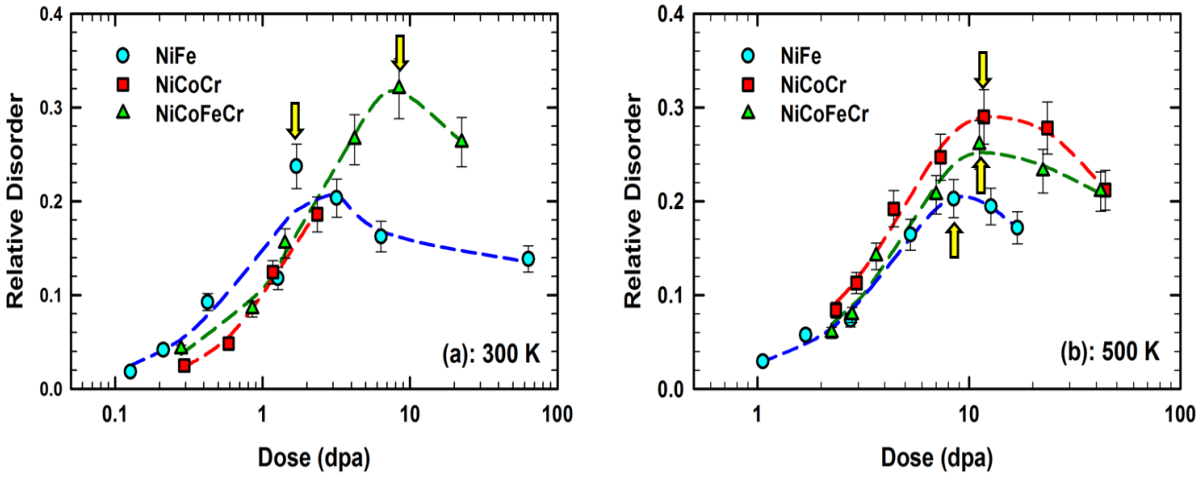

Fig. 8: Comparison of defect accumulation (relative disorder level at the initial damage peak vs. ion dose) in NiFe [73] (blue filled circles), NiCoCr [72] (red filled squares) and NiCoFeCr [76] (green filled triangles) irradiated with 1.5 MeV Ni ions at: (a) 300 K and (b) 500 K. The lines are curve fits to guide the eye.

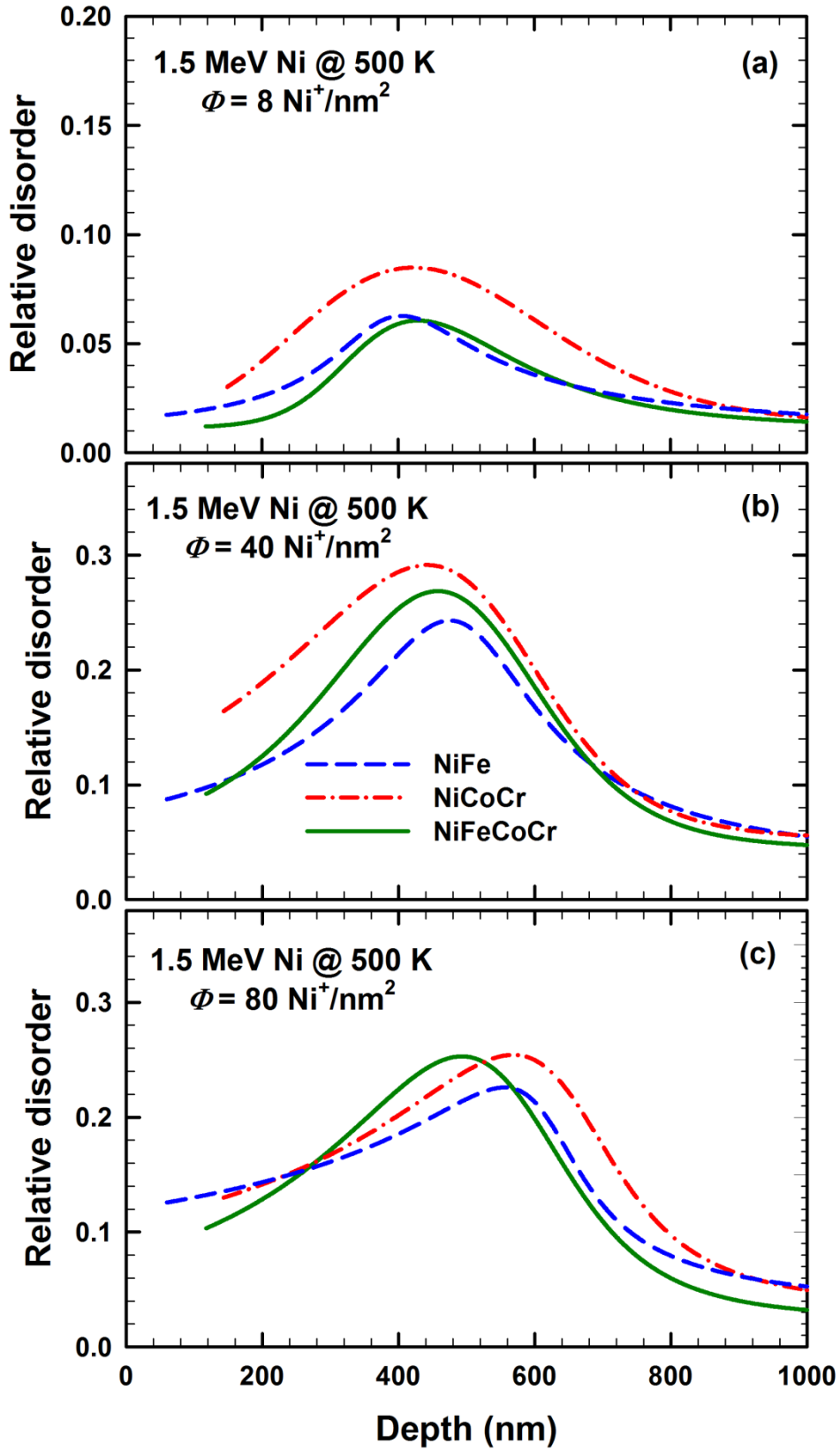

Fig. 9: Comparison of the relative disorder profiles for 1.5 MeV Ni-irradiated NiFe (blue dash line), NiCoCr (red dash-dot) and NiFeCoCr (gree solid line) at 500 K to fluence of (a) 8, (b) 40 and (c) 80 Ni^{+}/nm^{2}.The lines are the curves best fits to the data to guide the eye.